Advances in Sol-Gel Synthesis of $MgZr_{4(1-x)}Hf_{4x}P_6O_{24}$ (x = 0, 1) Solid Electrolytes for Electrochemical Devices

[1,2,3*]Mohammed Alhaji Adamu, [3]Girish M Kale
[1]Department of Metallurgical and Materials Engineering Technology, Kogi State Polytechnic, Lokoja, Kogi State, Nigeria
[2]Engineering Materials Research Group, Kogi State Polytechnic, Lokoja, Kogi State, Nigeria
[3]School of Chemical and Process Engineering, University of Leeds, Leeds LS2 9JT, United Kingdom
Corresponding Email: drmadamu@yahoo.com; Tel: +234(0)8057211707

Abstract
The potential solid electrolytes, $MgZr_4P_6O_{24}$ and $MgHf_4P_6O_{24}$ were prepared using modified novel sol-gel method. Structural and electrical properties of the solid electrolytes were determined. TGA-DSC analyses indicated that the pure dried xerogel powders, when calcined at 900 ºC converts to pure single phase $MgZr_4P_6O_{24}$ and $MgHf_4P_6O_{24}$ nanopowders with excellent crystallinity. Pellets of 13 mm diameter and 3.8 mm thickness made by uniaxial compression were respectively sintered at 1300 ºC. Powder XRD analyses indicated that crystalline phase of $MgZr_4P_6O_{24}$ and $MgHf_4P_6O_{24}$ nanoparticles exhibit monoclinic structure with crystallite size of approx. 39 mm and 42 mm, respectively. The sintered pellets were stable from 1000 ºC to 1300 ºC, with $MgHf_4P_6O_{24}$ solid electrolyte showing no trace of coexistent second phase at higher temperatures. Relative density analyses of sintered $MgZr_4P_6O_{24}$ and $MgHf_4P_6O_{24}$ pellets yield optimum density of approx. 99% and 98% at 1300 ºC, respectively, which are in perfect agreement with SEM-EDS analyses of the sintered pellets. Using impedance spectroscopy, the bulk ionic conductivity of the platinum-cured sintered $MgZr_4P_6O_{24}$ and $MgHf_4P_6O_{24}$ pellets were determined as 7.23 x 10^{-3} Scm^{-1} at 725 ºC and 4.52 x 10^{-4} Scm^{-1} at 747 ºC, respectively. Activation energy of $MgZr_4P_6O_{24}$ (E_a = 0.84±0.04eV) and $MgHf_4P_6O_{24}$ (E_a = 0.74±0.02eV) solid electrolytes indicating $MgZr_4P_6O_{24}$ solid electrolyte as possessing improved Mg^{2+}-ion conducting mobile species at high temperatures. However, both solid electrolytes find suitable applications in electrochemical devices.

Keywords: Sol-gel synthesis, Solid electrolyte, $MgZr_{4(1-x)}Hf_{4x}P_6O_{24}$, Structural analysis, Electrical Properties, Electrochemical devices

INTRODUCTION

Research in materials synthesis and characterisation shows the benefit of knowing the behaviour of materials in operation. Today, various materials function in both ambient and high temperature environment, as such, appropriate materials are selected for certain application. Selecting materials for high temperature application requires operational stability of relevant materials properties as well as environmental suitability compared to applications at ambient temperatures. Temperature influences the stability of functional materials in operation and the need to select materials suitable for different application is required.

Solid electrolytes are materials in which the electric current is predominantly by ions (Ipser *et al.,* 2010). They can be oxides, halides, sulphides and other types of solid materials. They have gained importance due to their role in various scientific and technological applications as they are being used in electrochemical cells to measure chemical potentials in gases, liquids and solids. In addition, they can also be used to control the chemical composition by coulometric titration. Theory of solid electrolytes and their applications, as observed in sensors and other electrochemical devices have been well discussed in many books (Hagenmuller & Van Gool, 1978; Subbarao, 1980; Rickert, 1982; Goto, 1988; Takehiko, 1989; Fischer & Janke, 1975; Hladik, 1972) and review papers (Pratt, 1990; Chang & Sommer, 1997; Kummer, 1972; Stevens & Binner, 1984; Collongues *et al.,* 1984; West, 1989; Ferloni & Magistris, 1994).

Solid electrolytes, like the magnesium zirconium phosphate, $MgZr_4P_6O_{24}$ and other phosphate-based solid electrolytes have been widely studied due to their potential applications as solid electrolytes in electrochemical devices and thermodynamic measurements (Kale & Jacob, 1989; Kale *et al.,* 1996; Mudenda & Kale, 2017). In the same light, data on the sol-gel synthesis and electrical characterisation of $MgZr_4P_6O_{24}$ solid electrolytes have been copiously published (Adamu & Kale, 2016; Adamu *et al.,* 2020; Kale *et al.,* 2004; Fergus, 2009; Pet'kov *et al.,* 2014). Recently, extensive attention have been given to $MgZr_4P_6O_{24}$ solid electrolyte owing to their simple preparation process, structural and thermal stability, ionic mobility and broad applications as ionic conductor in electrochemical devices. In comparison, data on sol-gel synthesis of the $MgHf_4P_6O_{24}$ solid electrolytes and

other phosphate electrolytes have been scarcely or not reported (Adamu & Kale, 2025a; Adamu & Kale, 2025b).

In this study, $MgHf_4P_6O_{24}$ solid electrolyte was prepared using sol-gel method akin to $MgZr_4P_6O_{24}$ solid electrolyte, because the sol-gel method has shown adequate potential in producing pure and fine homogeneous powders at a relatively low temperature, thereby reducing carbon footprint when compared to other available synthesis methods (Adamu & Kale, 2016; Adamu *et al.,* 2020; Kale *et al.,* 2004; Fergus, 2009; Pet'kov *et al.,* 2014; Kakihana, 1996). Furthermore, the sol-gel method used in producing this solid electrolyte provide potential advantage of achieving better homogeneity, better compositional control and lower processing temperature over conventional solid-state method, and this accounts for high relative density and improved ionic conductivity of the solid electrolytes (Mudenda & Kale, 2017; Adamu & Kale, 2016). In our recent study, sol-gel synthesis of the $MgZr_4P_6O_{24}$ solid electrolyte shows excellent improvement in the ionic mobility and conductivity of Mg^{2+}-ion conducting species in the solid electrolyte (Adamu & Kale, 2016; Adamu *et al.,* 2020). This could be attributed to the highly dense $MgZr_4P_6O_{24}$ solid electrolyte which invariably resulted in high ionic conducting solid electrolytes with improved ionic mobility of the conducting species.

Impedance spectroscopy measurement is a major characterisation requirement in this study. In obtaining a highly dense sample pellets, high sintering temperature is a conventional sintering practice for solid electrolytes. To obtain a pure stable phase pellet, the sintering temperature is carefully selected and since some composite pellets transform at relatively high-temperatures, the balance in sample pellet purity, stability and sintering temperatures has to be reached. For instance, the $MgZr_4P_6O_{24}$ sample compound transforms into $Zr_2(PO_4)_2O$ phase at a sintering temperature higher than 1300°C (Adamu & Kale, 2016), thereby changing the crystal structure or phase of the $MgZr_4P_6O_{24}$ solid electrolyte. However, $MgHf_4P_6O_{24}$ solid electrolyte maintains its stability at higher temperatures (Adamu & Kale, 2025a). One effect of heating a phosphate-based compound at a high temperature is the loss of P_2O_5 oxide from zirconia precipitate as a result of its volatility (Collin & Boilot, 1989).

The $MgZr_4P_6O_{24}$ and $MgHf_4P_6O_{24}$ solid electrolytes have likely applications in electrochemical devices like electrochemical sensors, solid-state Mg batteries and solid-oxide fuel cells (SOFCs).

MATERIALS AND METHOD

Materials preparation

All chemicals are analytical grade and used as received without further purification. Single phase $MgZr_{4(1-x)}Hf_{4x}P_6O_{24}$ (x = 0, 1) solid electrolytes were synthesised using sol-gel method to produce fine nanopowders; this was achieved through mixing on an atomic scale by combining aqueous solutions of precursor soluble salts at relatively low crystallisation temperature and, it produces chemical compositions that are not always possible by solid-state fusion method. Equation 1 and Equation 2 shows the stoichiometric amount of pure chemical solutions made from the precursors; $Mg(NO_3)_2$, $ZrOCl_2$ and $NH_4H_2PO_4$, to synthesis $MgZr_4P_6O_{24}$ xerogel powders (Adamu & Kale, 2016; Adamu *et al.,* 2020), while the precursors; $Mg(NO_3)_2$, $HfCl_4$ and $NH_4H_2PO_4$, in aqueous solutions were mixed separately in stoichiometric proportion to synthesis $MgHf_4P_6O_{24}$ xerogel powders. The resulting dried xerogel powders were calcined at 900 °C. The calcined nanopowders were then pelletised and sintered at 1300 °C, using data from TGA-DSC profiles. Furthermore, the sintered pellets of $MgZr_4P_6O_{24}$ and $MgHf_4P_6O_{24}$ solid electrolytes were characterised for their structural stability and electrical properties. The impedance analysis was determined using two-probe analysis at an impedance temperature ranging from 182 °C to 764 °C and a frequency ranging from 100 mHz to 32 MHz.

The sol-gel synthesis process illustrated in Figure 1 describes all the steps and chemical reactions involved in a sol-gel method; the steps such as preparing the sol (2) from inorganic precursors and monitored reaction (4) from which aqueous gel (6) was prepared which was dried during solvent evaporation (8) to form a dried xerogel powder (10) which was later calcined (11) at specific temperatures and annealing time to form the desired compound (12).

$$Mg(NO_3)_2\,(aq) + 4ZrOCl_2.8H_2O\,(aq) + 6NH_4H_2PO_4\,(aq) = \mathbf{MgZr_4P_6O_{24}\,(s)} + 6NH_4Cl\,(aq) + 2HCl\,(aq) + 2HNO_3\,(aq) + 36H_20\,(l) \quad \text{Equation 1}$$

(Adamu & Kale, 2016; Adamu *et al.,* 2020)

$$Mg(NO_3)_2\,(aq) + 4HfCl_4\,(aq) + 6NH_4H_2PO_4\,(aq) = \mathbf{MgHf_4P_6O_{24}\,(s)} + 6NH_4Cl\,(aq) + 10HCl\,(aq) + 2HNO_3\,(aq) \quad \text{Equation 2}$$

(Adamu & Kale, 2025a)

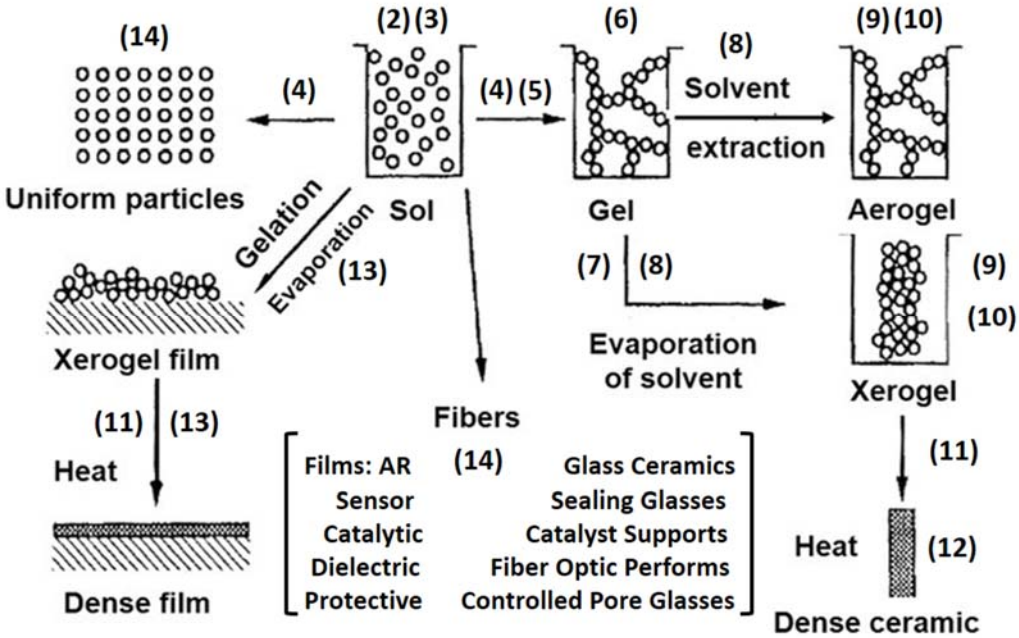

Figure 1: Sol-gel synthesis process showing all the steps of formation (Brinker & Scherer, 2013)

Materials characterisation

The STA 8000 (PerkinElmer, Seer Green, UK) was used to measure the TGA-DSC, which was later used to analyse the weight loss and thermal oxidation behaviour of the dried xerogel powders. In this measurement, effective optimisation calcination condition of the xerogel powders in a controlled atmosphere at a flow rate of 50 mL min^{-1} using a constant heating-cooling rate at 10 ºC min^{-1} within a temperature from 30 ºC to 1000 ºC, akin to that described in our recent paper (Adamu *et al.,* 2020). Based on the data from this measurement, the resultant dried xerogel powders were calcined at 900 ºC, and the pure calcined nano size powders were pelletised and sintered at 1300 ºC, using the same heating-cooling condition.

Powder x-ray diffractometer (Bruker D8 advance, Karlsruhe, GmbH) equipped with $CuK\alpha_1$ (λ = 1.5406 Å) radiation source operating at 30 kV and 45 mA and calibrated against Si standard was used to analyse the phase structure of $MgZr_4P_6O_{24}$ and $MgHf_4P_6O_{24}$ solid electrolytes. The x-ray diffraction data was collected over $10^o \leqslant 2\theta \leqslant 80^o$ scan range.

Some pellets of $MgZr_4P_6O_{24}$ and $MgHf_4P_6O_{24}$ solid electrolytes with 13 mm diameter and 3.8 mm thickness were pressed from their dried calcined nanopowders (mixed with 1 wt.% binder, Ciba Glascol HA4 and dried at 100 ºC for 0.5 h) using the room temperature compressive pressure consolidation of 5kN. The resultant green body-pellets were initially heated at 400 - 450 ºC for the purpose of burning off the Ciba Glascol HA4 binder prior sintering at different temperatures ranging from 1000 ºC to 1500 ºC for 24 h at 10 ºC min^{-1} heating rate. The resultant sintered pellets were characterised for their density.

Microstructure of the $MgZr_4P_6O_{24}$ and $MgHf_4P_6O_{24}$ solid electrolyte pellets were analysed using SEM (Carl Zeiss EVO MA15, Jena, GmbH) equipped with EDS and Oxford Aztec X-Act EDS spectrometer attached to Carl Zeiss EVO MA15 deployed for the elemental composition analysis of the pellets *in situ* at an accelerating voltage of 20 kV. The SEM images were obtained on a freshly broken surfaces of the pellets coated with a very thin platinum layer to avoid the pellets from charging.

Impedance analyser, Solartron SI1260 FRA (Hampshire, UK) was used to analyse the electrical properties of the solid electrolytes in this study. Sintered pellets of $MgZr_4P_6O_{24}$ and $MgHf_4P_6O_{24}$ solid electrolytes were mildly ground to achieve a flat surface area without diminishing the pellets thickness. Platinum paste (Sigma-Aldrich, UK) was lightly applied to the opposite parallel faces of the solid electrolytes sintered pellets, and then allowed to dry before firing in a tube furnace at 800 ºC for 0.5 h to form contact electrodes on both surfaces of the pellets. Ionic conductivity was therefore plotted as a function of temperature and frequency in the temperature range from 182 to 764 ºC and frequency range from 100 mHz to 32 MHz.

RESULTS AND DISCUSSIONS

Thermal analysis (TGA-DSC)

Figure 2 shows decomposition changes in $MgZr_4P_6O_{24}$ (Adamu & Kale, 2016; Adamu *et al.,* 2020) and $MgHf_4P_6O_{24}$ (Adamu & Kale, 2025a) xerogel powders using TGA-DSC profiles.

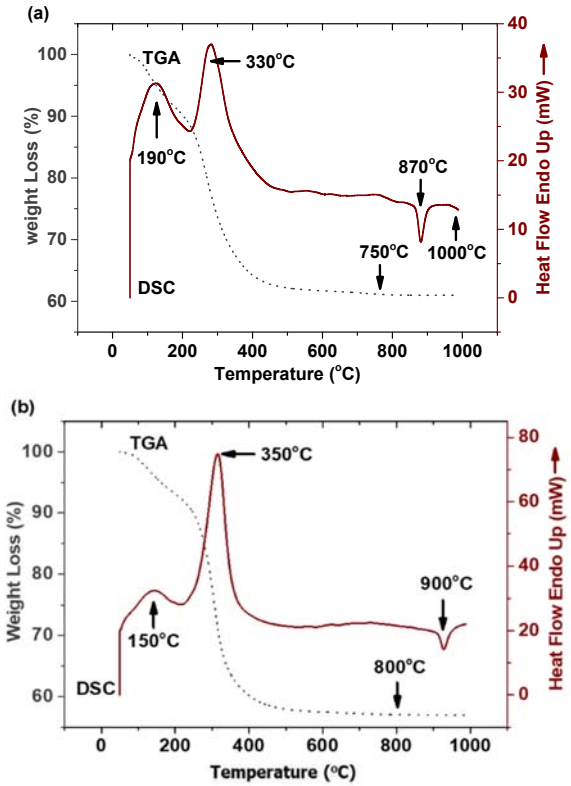

Figure 2: TGA-DSC profiles of (a) $MgZr_4P_6O_{24}$ (Adamu & Kale, 2016; Adamu *et al.,* 2020) (b) $MgHf_4P_6O_{24}$ (Adamu & Kale, 2025a) dried xerogel powders with a scan rate of 10 $^oCmin^{-1}$ in air

The TGA decomposition changes is presented in three different regions: The first region within 30 - 100 ºC corresponds to the removal of lattice H_2O. The weight loss in 150 - 500 ºC temperature region is attributed to the decomposition or oxidation of gelled inorganic precursor materials such as $Mg(NO_3)_2$, $HfCl_4$ and $NH_4H_2PO_4$. There was no further reduction in weight above 500±25 ºC for the $MgHf_4P_6O_{24}$ xerogel powders. Similarly, the DSC profiles of $MgHf_4P_6O_{24}$ xerogel powders clearly shows two endothermic decomposition peaks at 150 ºC and 350 ºC, and an exothermic peak at 900 ºC. It is also known that the inorganic precursor, $NH_4H_2PO_4$ decomposes into $(NH_4)_3H_2P_3O_{10}$ and H_2O molecules at 140 - 170 ºC which could be responsible for the endothermic peak at 150 ºC. $Mg(NO_3)_2$ compound also decomposes into MgO, NO_2 and O_2 at a temperature above 300 ºC, this could be responsible for the endothermic peak at 350 ºC. The reactive oxide HfO_2 formed by oxidation of $HfCl_4$ at 432 ºC yields $MgHf_4P_6O_{24}$ after stoichiometric composition reaction with MgO and P_2O_5 reactive oxides at 900 ºC. The exothermic peak observed at 900 ºC indicates the formation of a single phase $MgHf_4P_6O_{24}$ nanoparticles with full crystallinity. In this study, TGA-DSC analysis was limited to 1000 ºC because of the heating capacity range of the equipment.

According to the TGA-DSC analysis for $MgZr_4P_6O_{24}$ xerogel powders (Adamu & Kale, 2016; Adamu *et al.,* 2020) and for $MgHf_4P_6O_{24}$ (Adamu & Kale, 2025a) xerogel powders, a pure single phase of the respective solid electrolytes were formed at 800 ºC but fully crystallised at 900 ºC after calcination.

X-ray diffraction (XRD)

Figure 3 shows crystalline $MgZr_4P_6O_{24}$ and $MgHf_4P_6O_{24}$ nanopowders calcined at 900 ºC and the pellets sintered at 1300 ºC. In Figure 3(a) and Figure 3(b), it can be deduced that crystalline $MgZr_4P_6O_{24}$ and $MgHf_4P_6O_{24}$ solid electrolytes were formed at 900 ºC and the pellets were sintered at 1300 ºC, with no traces of coexistent second phase. However, in Figure 3(a), $MgZr_4P_6O_{24}$ sintered pellet shows minor extraneous peaks at higher temperatures, indicating coexistent second phase while Figure 3(b) shows no such traces. The profiles on Figure 3(a) and Figure 3(b) shows that the solid electrolyte is stable at 900 ºC which agrees with an earlier study (Kazakos-Kijowski *et al.,* 1988). In Figure 3(a) and Figure 3(b), the prepared solid electrolytes calcined and sintered at 900 ºC and 1300 ºC, respectively, were indexed against $Mg_{0.5}Zr_2(PO_4)_3$ [ICDD-04-016-0487] and $Zr_2(PO_4)_2O$ [ICDD-04-011-6948]. Figure 3(a) further revealed the minor second phase as an orthorhombic $Zr_2(PO_4)_2O$ compound at 22.54º 2θ which confirms that the sintered $MgZr_4P_6O_{24}$ solid electrolyte is stable at 1300 ºC (Adamu & Kale, 2016). Similarly, $MgHf_4P_6O_{24}$ nanopowders calcined at 900 ºC and sintered at 1300 ºC shows progressive stability as the sintering temperature increases. The diffraction spectra in Figure 3(a) and Figure 3(b) are similar in structure and they exhibit sharp peaks which indicates excellent crystallinities and long-range crystallographic orders (Zuttel, 2003). The similarity and lattice parameters of Zr and Hf analogues are of the same order because of the similarities in sizes and ionic radii, Zr^{4+} and Hf^{4+} [0.72Å and 0.71Å for six-fold coordination], respectively (Sugantha & Varadaraju, 1997; Shannon, 1976; Shannon & Prewitt, 1969). As stated in an earlier study, $MgZr_4P_6O_{24}$ solid electrolyte transforms from the monoclinic to orthorhombic $Zr_2(PO_4)_2O$ phase at temperatures higher than 1300 ºC (Adamu & Kale, 2016). However, $MgHf_4P_6O_{24}$ remains stable at higher temperatures but 1300 ºC was considered the sintering temperature for the purpose of thermal stability and reducing excess carbon footprint.

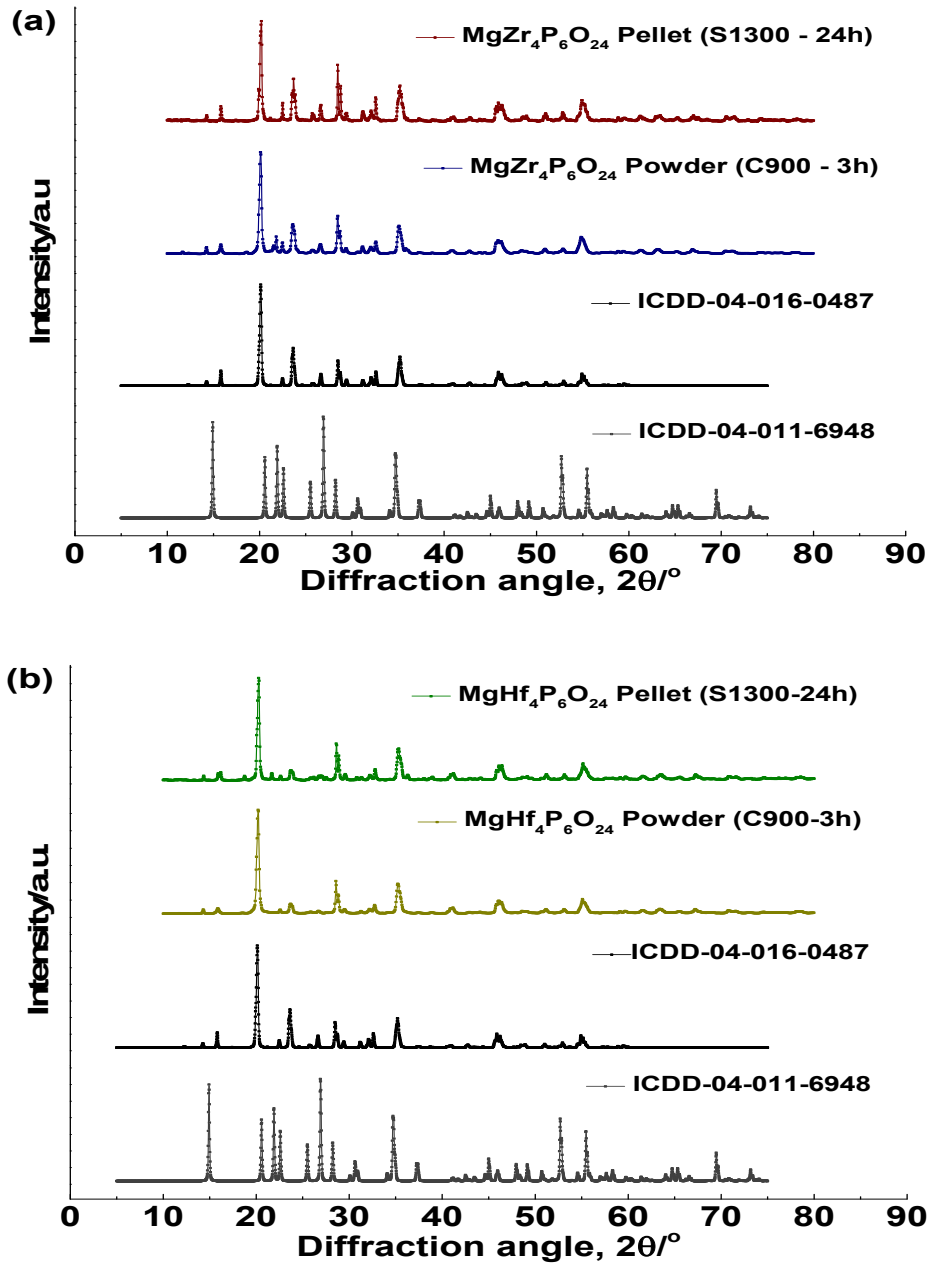

Figure 3: XRD profiles of (a) $MgZr_4P_6O_{24}$ (Adamu & Kale, 2016; Adamu *et al.,* 2020) (b) $MgHf_4P_6O_{24}$ (Adamu & Kale, 2025a) solid electrolytes nanopowders calcined at 900 ºC and pellets sintered at 1300 ºC. All profiles indexed to $Mg_{0.5}Zr_2(PO_4)_3$ [ICDD-04-016-0487] and $Zr_2(PO_4)_2O$ [ICDD-04-011-6948]

Density and porosity analyses

Figure 4 shows the dependence of relative density on sintering temperatures of $MgZr_4P_6O_{24}$ and $MgHf_4P_6O_{24}$ solid electrolytes. Figure 4(a) shows that the optimum relative density of approx. 99% and the least porosity of approx. 1% was achieved at a sintering temperature of 1300 ºC. The optimum relative density of approx. 99% for $MgZr_4P_6O_{24}$ solid electrolyte is in perfect agreement with an earlier study, that acceptable relative density of solid electrolytes should be higher than 94% (Mori *et al.,* 2006). Furthermore, the relative density of $MgZr_4P_6O_{24}$ solid electrolyte increases steadily from 60% to 99% as sintering temperature increases from 1000 ºC to 1300 ºC. At this sintering temperature, a maximum relative density of approx. 99% of the theoretical density was achieved as stable monoclinic system.

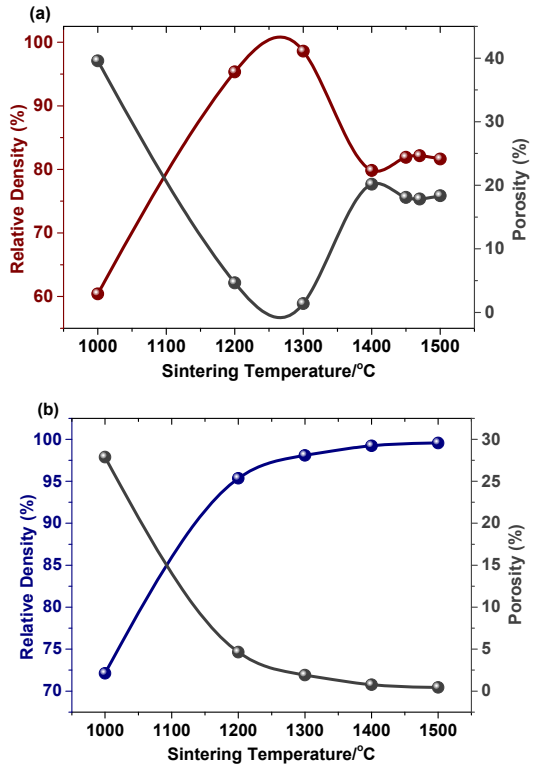

Figure 4: Dependence of relative density and porosity of (a) $MgZr_4P_6O_{24}$ (Adamu & Kale, 2016) (b) $MgHf_4P_6O_{24}$ (Adamu & Kale, 2025a) solid electrolytes on sintering temperature

The sintering temperatures from 1300 ºC to 1500 ºC shows significant transformation from monoclinic $MgZr_4P_6O_{24}$ to orthorhombic $Zr_2(PO_4)_2O$ phase which depicts a downward trend in the relative density from 99% to 82% at a sintering temperature of 1400 ºC. High volatility of P_2O_5 oxide at temperatures higher than 1300 ºC can be a contributing factor for the sharp decrease in density of $MgZr_4P_6O_{24}$ solid electrolyte, suggesting that 1300 ºC is the optimum sintering temperature. Figure 4 shows that porosity of solid electrolytes decreases with increasing sintering temperatures. This was observed in the sintering temperatures from 1000 ºC to 1300 ºC, where the porosity decreases rapidly from 40% to 1%. Similarly, $MgHf_4P_6O_{24}$ solid electrolyte presented in Figure 4(b) shows that the relative density increases steadily with sintering temperatures from 1000 ºC to 1500 ºC.

Figure 4(b) shows that the $MgHf_4P_6O_{24}$ solid electrolyte exhibit relative density of approx. 95% at temperatures higher than 1100 ºC and 98% optimum density at 1300 ºC. Furthermore, since the increment in relative density from 1300 ºC to 1500 ºC is approx. 1%, it suggests a saturation point has been reached for the densification of $MgHf_4P_6O_{24}$ solid electrolyte.

Morphology of solid electrolytes (SEM-EDS)

The morphological analyses of $MgZr_4P_6O_{24}$ and $MgHf_4P_6O_{24}$ solid electrolytes using SEM on a cross-section of fracture surface of the solid electrolytes pellets sintered at 1300 ºC are presented in Figure 5, equipped each with an EDS spectrum

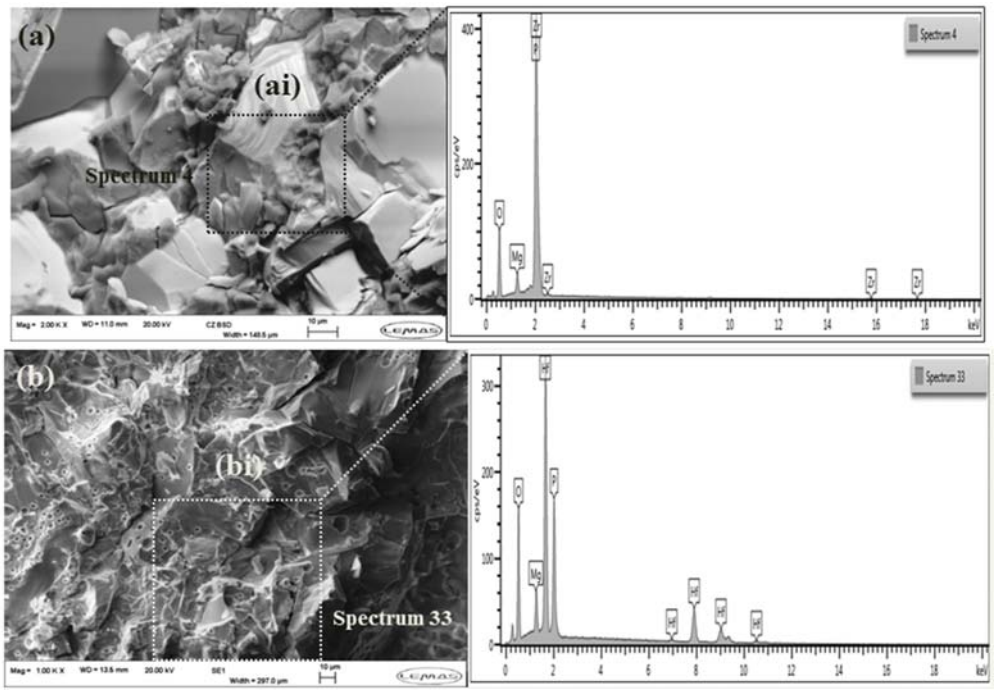

Figure 5: SEM micrographs fracture surfaces of (a) $MgZr_4P_6O_{24}$ (Adamu & Kale, 2016; Adamu *et al.,* 2020) (b) $MgHf_4P_6O_{24}$ pellets sintered at 1300 ºC, showing their corresponding EDS spectrum (ai - bi)

The elemental analysis, atomic fraction (%) and atomic ratio extracted from the EDS spectrum of the sintered $MgZr_4P_6O_{24}$ and $MgHf_4P_6O_{24}$ solid electrolyte pellets in Figure 5 is presented on Table 1.

Table 1: Average Elemental Composition of EDS Spectra from Fracture Surface of the Sintered $MgZr_4P_6O_{24}$ (Adamu & Kale, 2016; Adamu *et al.,* 2020) and $MgHf_4P_6O_{24}$ Solid Electrolyte Pellets

Element	Atomic Fraction (%)	Atomic Ratio
	$MgZr_4P_6O_{24}$	
Mg	2.83	1.00
Zr	11.68	4.13
P	16.53	5.84
O	68.96	26.13
Total	**100.00**	
	$MgHf_4P_6O_{24}$	
Mg	2.83	1.00
Hf	9.50	3.36
P	17.40	6.15
O	70.27	24.83
Total	**100.00**	

Figure 5 is micrographs of the $MgZr_4P_6O_{24}$ and $MgHf_4P_6O_{24}$ solid electrolyte fracture surface pellets sintered at 1300 ºC. Figure 5(a) and Figure 5(b) shows that both sintered pellets possess dense structure which is in perfect agreement with the relative densities of $MgZr_4P_6O_{24}$ (99%) and $MgHf_4P_6O_{24}$ (98%) solid electrolytes, respectively. It also shows that the fracture mode are almost totally intergranular and that there are no secondary phases observed at the grain boundaries or segregation to the grain boundaries.

The EDS points analysed from a number of sites show that both solid electrolytes are homogeneous and the average elemental composition from different locations for $MgZr_4P_6O_{24}$ solid electrolyte have stoichiometric concentration. However, the elemental composition of some points for $MgHf_4P_6O_{24}$ solid electrolyte are non-stoichiometric because the atomic ratio of some elements shown on Table 1 are much smaller than the required standard hence, they could not be standardised by approximation.

Figure 6 is EDS mapping across the fracture surfaces of sintered $MgZr_4P_6O_{24}$ and $MgHf_4P_6O_{24}$ solid electrolyte pellets showing the homogeneity of the various component oxides and possible phase reactions.

The EDS elemental mapping across the fracture surfaces of $MgZr_4P_6O_{24}$ and $MgHf_4P_6O_{24}$ solid electrolytes presented in Figure 6 shows a clear identification of the component elements in the map spectrum of the two solid electrolytes analysed in this study. The different component elements further shows the stoichiometric chemical relation defined by atomic ratio of the solid electrolytes. The component maps presented in different colours are reflective of the EDS layered image. In Figure 6(a), the presence of Mg, Zr, P and O are clearly identified on the EDS layered image in different colours which shows that the sample component analysed is homogeneous. Similarly, the elemental maps distribution of $MgHf_4P_6O_{24}$ solid electrolyte is described in Figure 6(b). In both cases, all the component elements were distinguished with clear unique colours corresponding to their homogeneous distribution on the EDS layered images.

Temperature dependence of ionic conductivity

Figure 7 shows ionic conductivity of $MgZr_4P_6O_{24}$ and $MgHf_4P_6O_{24}$ solid electrolytes as a function of temperature. In this study, several points are outlined: Firstly, the linearity of the plots suggest there are no significant structural and phase changes noticed in the impedance temperatures. This identifies $MgZr_4P_6O_{24}$ and $MgHf_4P_6O_{24}$ solid electrolytes as having comparable ionic conducting species. Activation energy (E_a) which is energy of formation and migration of ions in $MgZr_4P_6O_{24}$ and $MgHf_4P_6O_{24}$ solid electrolytes were analysed from the gradient of Arrhenius plots by fitting the ionic conductivity data in this study with Arrhenius equation presented in Equation 3

$$\sigma T = \sigma_o(T)\exp\left(-\frac{E_a}{kT}\right) \qquad \text{Equation 3}$$

where:

σ_o = Pre-exponential factor related to the effective number of mobile charge carriers

E_a = Thermal activation energy for oxide ion migration

T = Absolute temperature (in Kelvin, K)

k = Boltzmann constant

Ionic conduction is a thermally activated transport process. Therefore, the ionic conductivity of a solid electrolyte increases at increasing temperatures (Zuttel, 2003; Bellino *et al.,* 2006; Prabu *et al.,* 2011). In this study, ionic conductivity of $MgZr_4P_6O_{24}$ and $MgHf_4P_6O_{24}$ solid electrolytes increase exponentially as temperatures increase. The ionic conductivity of $MgZr_4P_6O_{24}$ and $MgHf_4P_6O_{24}$ solid electrolytes and

their corresponding impedance temperatures in Figure 7 are 7.23 x 10^{-3} Scm^{-1} at 725 ºC and 4.52 x 10^{-4} Scm^{-1} at 747 ºC, respectively, and their respective activation energy (E_a) from the slope of $\ln\sigma_{dc}T$ - $1000T^{-1}$ plots in Figure 7 are 0.84±0.04 eV and 0.74±0.02 eV. This indicates that $MgZr_4P_6O_{24}$ solid electrolyte exhibits a higher conductivity (σ_{ac} = 7.23 x 10^{-3} Scm^{-1}) at 725 ºC while $MgHf_4P_6O_{24}$ solid electrolyte has a higher mobility of Mg^{2+}-ions at 747 ºC. The ionic conductivity of both solid electrolytes in Figure 7 shows that $MgZr_4P_6O_{24}$ solid electrolyte analysed from 197 ºC to 725 ºC portrays better ionic conducting species than $MgHf_4P_6O_{24}$ solid electrolyte analysed from 182 ºC to 747 ºC. However, the $MgHf_4P_6O_{24}$ solid electrolyte maintains better thermal stability at temperatures higher than 1300 ºC. Furthermore, it was observed that the crossover point in Figure 7 for the bulk ionic conductivity is identified at 394 ºC. This suggests that $MgZr_4P_6O_{24}$ solid electrolyte is a marginally better ionic conductor than $MgHf_4P_6O_{24}$ solid electrolyte at temperatures greater than 394 ºC whereas, at temperatures below 394 ºC, $MgHf_4P_6O_{24}$ solid electrolyte is marginally better than $MgZr_4P_6O_{24}$ solid electrolyte. This observation could be as a result of the enhancement of ionic conductivity due to space-charge region effect (Vaidehi *et al.,* 1986) since the $MgZr_4P_6O_{24}$ solid electrolyte is a composite solid electrolyte while $MgHf_4P_6O_{24}$ solid electrolyte is a single-phase solid electrolyte.

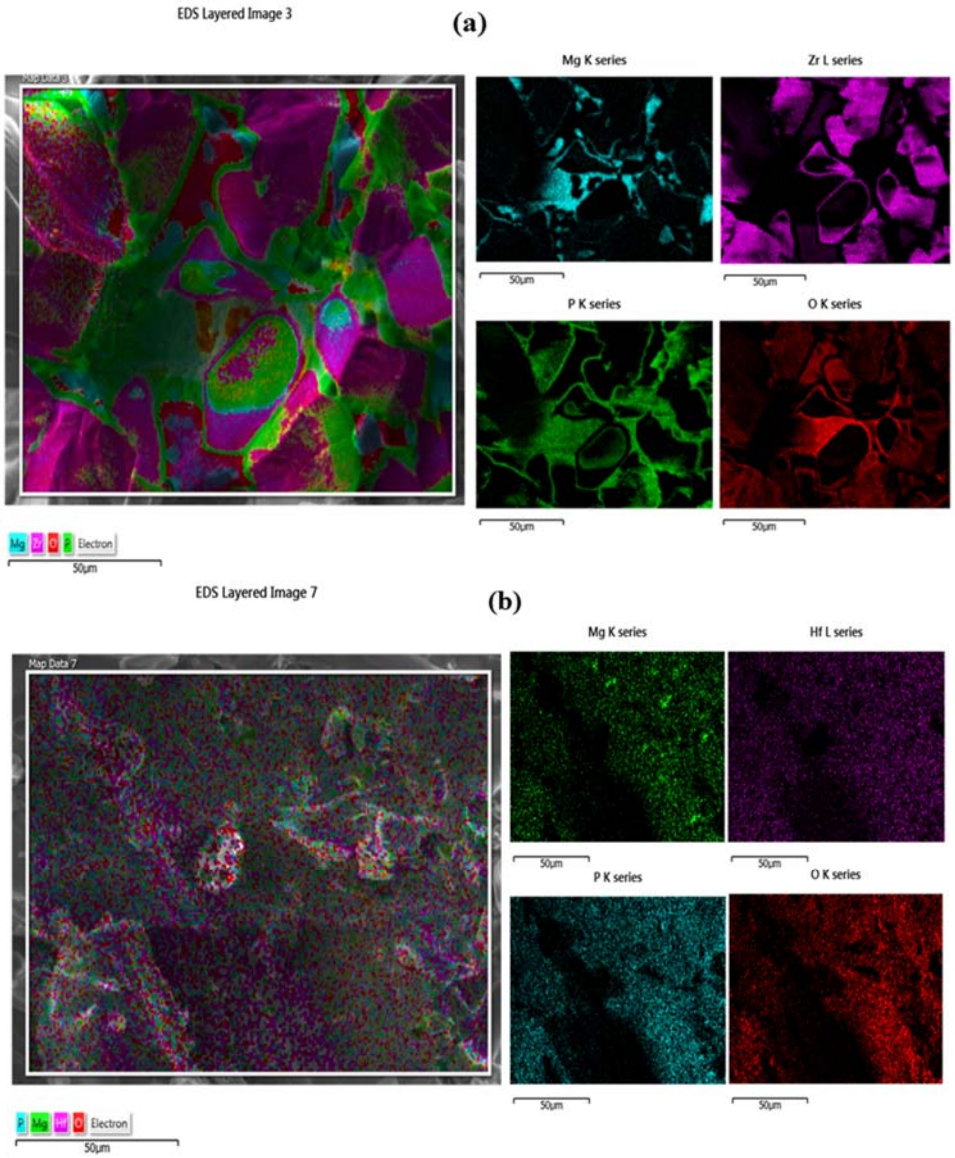

Figure 6: EDS mapping across the fracture surface of (a) $MgZr_4P_6O_{24}$ (b) $MgHf_4P_6O_{24}$ solid electrolyte pellets sintered at 1300 ºC

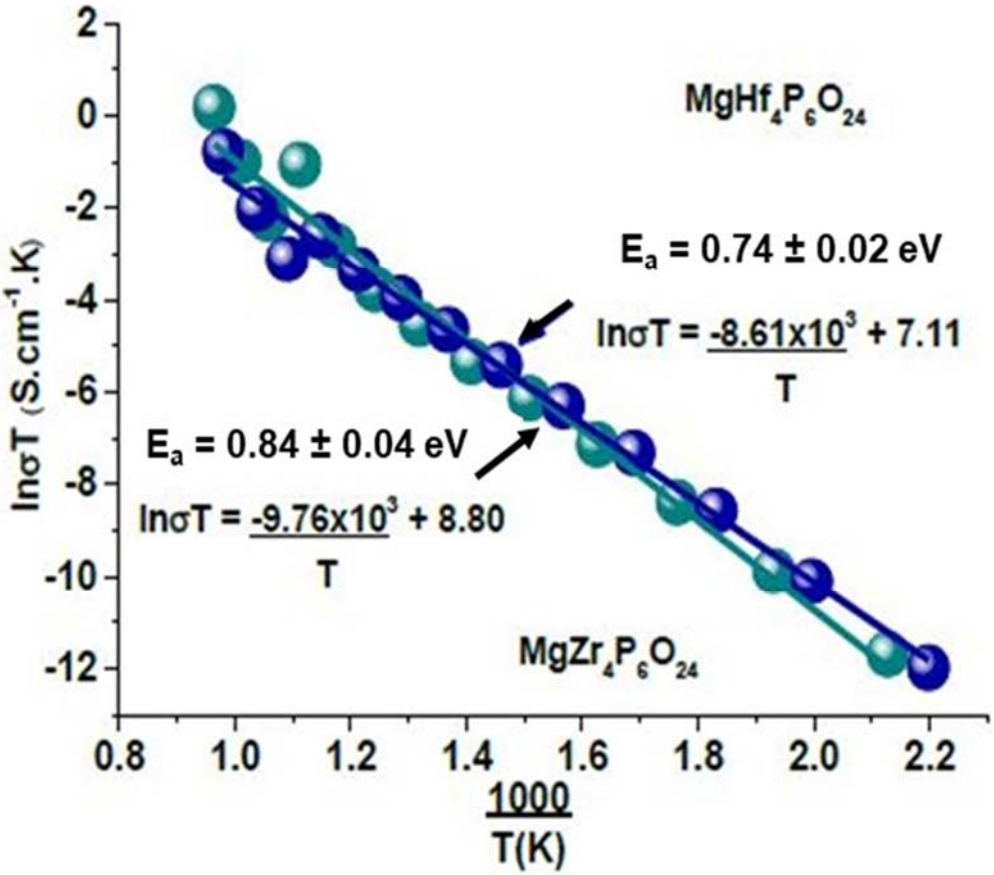

Figure 7: Bulk ionic conductivity profiles of $MgZr_4P_6O_{24}$ (Adamu & Kale, 2016; Adamu *et al.,* 2020) and $MgHf_4P_6O_{24}$ (Adamu & Kale, 2025a) solid electrolytes as a function of temperature

CONCLUSION

According to TGA-DSC and XRD analyses, the xerogel powders prepared during sol-gel synthesis transformed to pure single phase monoclinic $MgZr_4P_6O_{24}$ and $MgHf_4P_6O_{24}$ solid electrolytes after calcination at 900 ºC. Dense and stable pellets of $MgZr_4P_6O_{24}$ and $MgHf_4P_6O_{24}$ solid electrolytes for density, morphology and impedance analyses were prepared by room temperature compressive pressure consolidation and sintering of the calcined nano size powders at 1300 ºC. The electrical properties of $MgZr_4P_6O_{24}$ and $MgHf_4P_6O_{24}$ solid electrolytes were determined as a function of temperature using impedance spectroscopy. The solid electrolytes appear to be Mg^{2+}-ion conductor at high temperatures for electrochemical devices and thermodynamic measurements.

ACKNOWLEDGEMENTS

We appreciate Kogi State Polytechnic and Tertiary Education Trust Fund (TETFund) for providing infrastructure and funding opportunities for this study. We also thank the School of Chemical and Process Engineering, University of Leeds, Leeds LS2 9JT, United Kingdom for providing world class laboratories and workshops for this study.

REFERENCES

Adamu, M., & Kale, G. M. (2016). Novel sol-gel synthesis of $MgZr_4P_6O_{24}$ composite solid electrolyte and newer insight into the Mg^{2+}-ion conducting properties using impedance spectroscopy. *Journal of Physical Chemistry C*, 120(32), 17909-17915.

Adamu, M., Jacob, K. T., & Kale, G. M. (2020). Assessment of $MgZr_4P_6O_{24}$ solid electrolyte for sensing Mg in molten non-ferrous alloys. *Journal of The Electrochemical Society,* 167, 027532.

Adamu, M. A., & Kale, G. M. (2025a). Structural and thermal stability of sol-gel prepared

$MgHf_4P_6O_{24}$ solid electrolyte in molten pure aluminium. International *Journal of Recent Innovations in Academic Research,* 9(3)**,** 294-300.

Adamu, M. A., & Kale, G. M. (2025b). Electrical and electrochemical characterisation of sol-gel prepared Magnesium Hafnium Phosphate solid electrolyte for magnesium-sensors. International *Journal of Recent Innovations in Academic Research,* 9(3)**,** 337-344.

Bellino, M. G., Lamas, D. G., & Walsoe de Reca, N. E. (2006). A mechanism for the fast ionic transport in nanostructured oxide-ion solid electrolytes. *Advanced Materials,* 18(22), 3005-3009.

Brinker, C. J., & Scherer, G. W. (2013). Sol-gel science: the physics and chemistry of sol-gel processing. Academic Press, New York, 912.

Chang, Y. A., & Sommer, F. (1997). Thermodynamics of alloy formation, in: *TMS* 1997. Warrendale, 77.

Collin, G., & Boilot, J. P. (1989). Superionic solids and solid electrolytes. Academic Press, San Diego.

Collongues, R., Gourier, D., Kahn, A., Boilot, J. P., Colomban, Ph., & Wicker, A. (1984). β alumina, a typical solid electrolyte: latest developments in fundamental approach and in battery utilsation. *Journal of Physics and Chemistry of Solids,* 45(10), 981-1013.

Fergus, J. W. (2009). Electrochemical sensors: fundamentals, key materials and applications. solid state electrochemistry I: fundamentals, materials and their applications, 427-491.

Ferloni, P., & Magistris, A. (1994). New materials for solid state electrochemistry. *Journal de Physique IV France,* C1-3-C1-15.

Fischer, W. A., & Janke, D. (1975). Metallurgische elektrochemie. Verlag Stahleisen, Dusseldorf.

Goto, K. S. (1988). Solid state electrochemistry and its applications to sensors and electronic devices. Elsevier, Amsterdam.

Hagenmuller, P., & Van Gool, W. (1978). Solid electrolytes: general principles, characterisation, materials, applications. Academic Press, New York.

Hladik, J. (1972). Physics of electrolytes: thermodynamics and electrode processes in solid-state electrolytes (Vol. 2). Academic Press, London.

Ipser, H., Mikula, A., & Katayama, I. (2010). Overview: the emf method as a source of experimental thermodynamic data. *Calphad,* 34(3), 271-278.

Kakihana, M. (1996). Invited review 'sol-gel' preparation of high temperature superconducting oxides. *Journal of Sol-Gel Science and Technol*ogy, 6(1), 7-55.

Kale, G. M., & Jacob, K. T. (1989). Thermodynamic partial properties of Na_2O in NASICON solid solution, $Na_{1+x}Zr_2Si_xP_{3-x}O_{12}$. *Journal of Materials Research,* 4(2), 417-422.

Kale, G. M., Davidson, A. J., & Fray, D. J. (1996). Investigation into an improved design of CO_2 sensor. *Solid State Ionics,* 86-88, 1107-1110.

Kale, G. M., Wang, L., & Hong, Y. (2004). High-temperature sensor for in-line monitoring of Mg and Li in molten Al employing ion-conducting ceramic electrolytes. *International Journal of Applied Ceramic Technology,* 1(2), 180-187.

Kazakos-Kijowski, A., Komarneni, S., Agrawal, D., & Roy R. (1988). Synthesis, crystal data and thermal stability of Magnesium Zirconium Phosphate $[MgZr_4(PO_4)_6]$. *Materials Research Bulletin,* 23(8), 1177-1184.

Kummer, J. T. (1972). β-alumina electrolytes. *Progress in Solid State Chemistry,* 7, 141-175.

Mori, M., Suda, E., Pacaud, B., Murai, K., & Moriga, T. (2006). Effect of components in electrodes on sintering characteristics of $Ce_{0.9}Gd_{0.1}O_{1.95}$ electrolyte in intermediate-temperature solid oxide fuel cells during fabrication. *Journal of Power Sources,* 157(2), 688-694.

Mudenda, S., & Kale, G. M. (2017). Electrochemical determination of activity of Na_2O in $Na_2Ti_6O_{13}$-TiO_2 two phase system between 803-1000 K. *Electrochimica Acta,* 258, 1059-1063.

Pet'kov, V. I., Shipilov, A. S., Markin, A. V., & Smirnova, N. N. (2014). Thermodynamic properties of crystalline Magnesium Zirconium Phosphate. *Journal of Thermal Analysis and Calorimetry,* 115(2), 1453-1463.

Prabu, M., Selvasekarapandian, S., Kulkarni, A. R., Karthikeyan, S., Hirankumar, G., & Sanjeeviraja, C. (2011). Ionic transport properties of $LiCoPO_4$ cathode material. *Solid State Sciences,* 13(9), 1714-1718.

Pratt, J. (1990). Applications of solid electrolytes in thermodynamic studies of materials: a review. *Metallurgical and Materials Transactions A,* 21(5), 1223-1250.

Rickert, H. (1982). Electrochemistry of solids: an introduction. Springer-Verlag, Berlin.

Shannon, R. D. (1976). Revised effective ionic radii and systematic studies of interatomic distances in halides and chalcogenides. *Acta Crystallographica. Section A*: *Crystal Physics Diffraction, Theoretical and General Crystallography,* 32(5), 751-767.

Shannon, R. T., & Prewitt, C. T. (1969). Effective ionic radii in oxides and fluorides. *Acta Crystallographica B: Structural Science,*

Crysta Engineering and Materials, 25(5), 925-946.

Stevens, R., & Binner, J. (1984). Structure, properties and production of β-alumina. *Journal of Materials Science,* 19(3), 695-715.

Subbarao, E. C. (1980). Solid electrolytes and their applications. Plenum Press, New York.

Sugantha, M., & Varadaraju, U. (1997). Ionic conductivity of Li^{+}-ion conductors $Li_2M^{3+}M^{4+}P_3O_{12}$. *Solid State Ionics,* 95(3), 201-205.

Takehiko, T (ed). (1989). High conductivity solid ionic conductors: recent trends and applications. World Scientific, Hong Kong.

Vaidehi, N., Akila, R., Shukla, A. K., & Jacob, K. T. (1986). Enhanced ionic conduction in dispersed solid electrolyte systems CaF_2 Al_2O_3 and CaF_2 CeO_2. *Materials Research Bulletin,* 21(8), 909-916.

West, A. R. (1989). Solid electrolytes. *Ber. Bunsenges. Physical Chemistry,* 93(11), 1235-1241.

Züttel, A. (2003). Materials for hydrogen storage. *Materials Today,* 6(9), 24-33.